Acta Crystallographica Section F
Structural Biology and Crystallization Communications
ISSN 1744-3091

Crystallization of an atypical short-chain dehydrogenase from *Vibrio vulnificus* lacking the conserved catalytic tetrad

Geraldine Buysschaert, Kenneth Verstraete, Savvas N. Savvides* and Bjorn Vergauwen*

Unit for Structural Biology, Laboratory for Protein Biochemistry and Biomolecular Engineering (L-ProBE), Unit for Structural Biology, Ghent University, K. L. Ledeganckstraat 35, B-9000 Ghent, Belgium

Correspondence e-mail: savvas.savvides@ugent.be, bjorn.vergauwen@ugent.be

Received 14 March 2012
Accepted 25 April 2012

Short-chain dehydrogenases/reductases (SDRs) are a rapidly expanding superfamily of enzymes that are found in all kingdoms of life. Hallmarked by a highly conserved Asn-Ser-Tyr-Lys catalytic tetrad, SDRs have a broad substrate spectrum and play diverse roles in key metabolic processes. Locus tag VVA1599 in *Vibrio vulnificus* encodes a short-chain dehydrogenase (hereafter referred to as SDRvv) which lacks the signature catalytic tetrad of SDR members. Structure-based protein sequence alignments have suggested that SDRvv may harbour a unique binding site for its nicotinamide cofactor. To date, structural studies of SDRs with altered catalytic centres are underrepresented in the scientific literature, thus limiting understanding of their spectrum of substrate and cofactor preferences. Here, the expression, purification and crystallization of recombinant SDRvv are presented. Two well diffracting crystal forms could be obtained by cocrystallization in the presence of the reduced form of the phosphorylated nicotinamide cofactor NADPH. The collected data were of sufficient quality for successful structure determination by molecular replacement and subsequent refinement. This work sets the stage for deriving the identity of the natural substrate of SDRvv and the structure–function landscape of typical and atypical SDRs.

1. Introduction

Vibrio vulnificus is a naturally occurring Gram-negative bacterium that colonizes coastal marine environments. The ingestion of raw contaminated seafood such as oysters and clams or the exposure of open wounds to infected water can lead to rapidly progressing fatal septicaemia or tissue necrosis, respectively. *V. vulnificus* is closely related to the causative agent of cholera and is responsible for the majority of reported seafood-related deaths in the United States (Jones & Oliver, 2009).

Genome analysis of this human pathogen revealed the presence of 25 genes coding for short-chain dehydrogenases (abbreviated as SDRs). SDRs form an omnipresent and growing family of NAD(P)-dependent oxidoreductases that are distinct from the functionally related medium-chain dehydrogenases/reductases (MDRs) and aldo–keto reductases by their sequence length and characteristic sequence motifs (Filling *et al.*, 2002). SDRs are functionally diverse and have been linked to a multitude of substrates, involving them in many important cellular processes as diverse as sugar and nucleotide metabolism, steroid and hormone metabolism, redox sensing and phase I metabolism of many endogenous (biogenic aldehydes and reactive lipid-peroxidation products) and xenobiotic (pharmacological drugs, carcinogens and toxicants) compounds (Oppermann & Maser, 2000; Kavanagh *et al.*, 2008; Hoffmann & Maser, 2007). Despite rather low pairwise sequence identities between members of the superfamily, typically in the range 15–30%, SDRs demonstrate a well conserved tertiary architecture (Kallberg *et al.*, 2002). Members of the SDR superfamily are structurally classified as open-twisted α/β proteins featuring the Rossmann dinucleotide-binding motif (Rossmann *et al.*, 1974). Consistent with the observed weak mutual sequence similarity, classical SDRs only have a handful of strictly

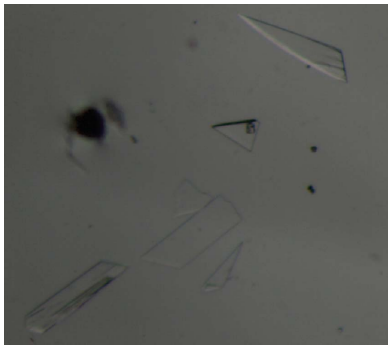

conserved residues, which appear at the core of the structure and in the Rossmann fold and aid in catalysis and cofactor stabilization, respectively. Nearly all classical SDRs use the conserved Asn-Tyr-Lys-Ser motif as catalytic residues, whereas a Gly-*X*-*X*-*X*-Gly-*X*-Gly motif is retained in the Rossmann fold to accommodate the adenine nucleotide diphosphate of the cofactor.

The product of the *V. vulnificus* YJ016 locus tag VVA1599, SDRvv, clusters within the 'classical' SDR family, as does the top homologue identified by *BLAST* analysis of structurally characterized SDRs: the *Escherichia coli* enoyl reductase FabG. Based on protein sequence alignments, however, SDRvv clearly lacks the active-site residues that facilitate hydride transfer in this family of oxidoreductases. Among these are the Tyr and Lys residues of the catalytic tetrad, which are also crucial for cofactor binding as they engage in hydrogen bonding to the hydroxyl groups of the nicotinamide ribose. The Tyr→Lys and Lys→Asn substitutions observed in SDRvv therefore must abrogate catalytic proficiency. In addition to the absence of the catalytic tetrad, well conserved amino acids shown to be important for catalysis by mutagenesis studies, such as, for example, a Thr and the NNAG motif at positions 10 and 85–88, respectively, in *E. coli* FabG (PDB entry 1q7b; Price *et al.*, 2004), are also not retained in SDRvv (Filling *et al.*, 2002). Furthermore, the Rossmann fold of SDRvv appears to be truncated, lacking a large piece of the loop that joins helices α2 and α3.

Here, we report the expression, isolation and preliminary crystallographic studies of recombinant SDRvv in the apo form and in complex with its cofactor NADPH. Crystals were obtained in cocrystallization experiments with NADPH and one crystal form showed unbiased difference density that clearly demonstrated the presence of bound NADPH cofactor at full occupancy. Therefore, this work identifies and delineates the reducing cofactor conformation of the 'classical' family outlier SDRvv from *V. vulnificus*.

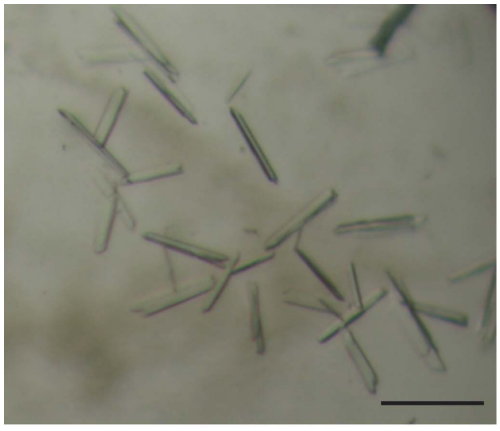

(*a*)

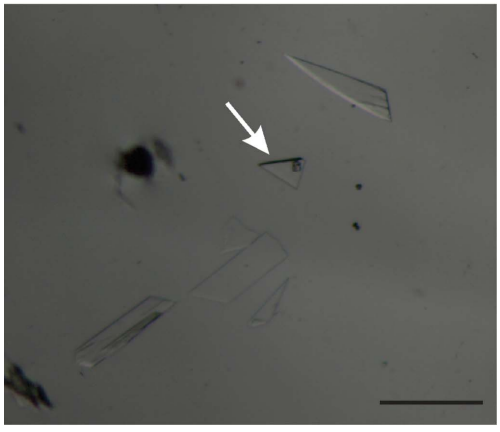

(*b*)

Figure 1
Single crystals of human SDRvv from *V. vulnificus* cocrystallized with NADPH using the sitting-drop vapour-diffusion method and belonging to the primitive monoclinic space group $P2_1$. (*a*) Crystals that appeared in 0.2 *M* ammonium acetate, 0.1 *M* bis-Tris pH 6.5, 25% PEG 3350 and referred to as crystals with morphology *A* (SDRvv-*A*). The scale bar is 50 µm in length. (*b*) Typical crystals grown in 0.1 *M* bis-Tris pH 6.5, 18% PEG 5000 for 2 d. The triangular-shaped crystal indicated with an arrow is referred to as a crystal with morphology *B* (SDRvv-*B*). The scale bar is 100 µm in length.

2. Experimental procedures

2.1. Cloning and expression

The open reading frame *VVA1599* encoding SDRvv from *V. vulnificus* YJ016 (accession No. NC_005140) was synthesized and inserted into the pUC18 plasmid (GenScript Corporation, Piscataway, New Jersey, USA). To facilitate cloning procedures into the T7-inducible expression vector pACYCDuet-I (Novagen), unique *Nde*I and *Kpn*I restriction sites were introduced at the N- and C-termini by PCR amplification using the sense and antisense primers 5′-CATATGATGGGATCAGACAAAACCG-3′ and 5′-GGTACCCTAACCCAGCAGCGCGCC-3′, respectively. Since the native stop codon is retained, SDRvv will be recombinantly expressed in its native state, *i.e.* without an affinity tag.

Electrocompetent *E. coli* BL21 (DE3) cells were transformed with pACYCDuet-I-VVA1599 and cultured with continuous shaking at 310 K in Luria–Bertani medium supplemented with chloramphenicol. Fully grown overnight precultures were subsequently diluted in fresh medium (at a 1:100 ratio) and induced for expression by the addition of a final concentration of 1 m*M* IPTG when an optical density (OD_{600}) of 0.6 was reached. After induction, cells were grown for a minimum of 4 h in a rotary shaker at 310 K and were harvested by centrifugation at 4000*g* for 30 min at 277 K. Cell pellets were resuspended in buffer *A* (50 m*M* Tris pH 8.5) and lysed by sonication.

2.2. Protein purification

SDRvv was purified to homogeneity using a three-step procedure. Firstly, the SDRvv-enriched lysate was loaded under gravity onto a Q-Sepharose Fast Flow column pre-equilibrated with buffer *A*. The protein was eluted with an increasing concentration of NaCl in steps of 100 m*M*. Fractions containing recombinant protein were pooled and buffer-exchanged by dialysis against buffer *B* (50 m*M* Tris pH 7.2). A second round of anion-exchange chromatography was applied using a SourceQ column connected to an ÄKTA system (GE Healthcare). Bound protein was eluted using a linear NaCl gradient and was concentrated prior to size-exclusion chromatography (SEC; HiLoad 26/60 Superdex 200 column, GE Healthcare). SEC was performed using 50 m*M* Tris pH 8.0, 150 m*M* NaCl as the eluting buffer. The observed elution volume of the single SDRvv peak was consistent with the predicted molecular weight of a tetramer (94 616 Da). At every stage, the purity of SDRvv was monitored by SDS–PAGE. The molecular weight and the identity of the purified protein was further confirmed by MALDI–TOF mass spectrometry using peptide mass fingerprinting.

2.3. Crystallization and data collection

Purified SDRvv was concentrated to 8 mg ml^{-1} using centrifugal microconcentrators (10 kDa molecular-weight cutoff; Centricon) and

Table 1
Crystal data and data-collection statistics.

Values in parentheses are for the highest resolution shell.

	SDRvv-*A*	SDRvv-*B*
Date	June 12, 2011	July 18, 2011
Beamline	PROXIMA1, SOLEIL	X06SA, SLS
Detector	ADSC Q315	Pilatus 6M
Temperature (K)	100	100
Wavelength (Å)	0.98011	0.99993
No. of crystals	1	1
Oscillation range per image (°)	0.5	0.2
Total oscillation range (°)	180	180
Resolution range (Å)	45.0–2.35 (2.49–2.35)	40.0–1.80 (1.91–1.80)
Space group	$P2_1$	$P2_1$
Unit-cell parameters (Å, °)	a = 59.37, b = 122.89, c = 63.14, β = 111.09	a = 69.63, b = 96.26, c = 72.11, β = 103.99
No. of observed reflections	127883 (19059)	288963 (45106)
No. of unique reflections	34318 (5346)	84971 (13354)
Multiplicity	3.7 (3.6)	3.4 (3.4)
Data completeness (%)	97.0 (94.3)	99.1 (97.0)
$R_{\rm meas}$† (%)	13.1 (68.4)	9.5 (56.1)
Mean $I/\sigma(I)$	10.6 (2.7)	10.5 (2.4)
Mosaicity (°)	0.4	0.2
Wilson B (Å^2)	29	19
No. of molecules in asymmetric unit	4	4
Solvent content‡ (%)	45.8	50.4
Matthews coefficient‡ (Å^3 Da^{-1})	2.3	2.5

† $R_{\rm meas} = \sum_{hkl}\{N(hkl)/[N(hkl)-1]\}^{1/2}\sum_i |I_i(hkl) - \langle I(hkl)\rangle|/\sum_{hkl}\sum_i I_i(hkl)$, where N is the multiplicity, $I_i(hkl)$ is the intensity of the ith measurement of reflection hkl and $\langle I(hkl)\rangle$ is the average value over multiple measurements (Diederichs & Karplus, 1997). ‡ Estimates of solvent contents and Matthews coefficients were calculated using *Matthews Probability Calculator* (http://www.ruppweb.org/mattprob/; Kantardjieff & Rupp, 2003; Matthews, 1968).

complexed with its corresponding nucleotide cofactor by addition of a molar excess of NADPH (1 m*M*). This particular ligand was chosen on the basis of fluorescence-based thermal shift assays (probing oxidized and reduced forms of NAD and NADP; data not shown) and because of the presence of an Arg in the putative $\beta_2\alpha_3$ turn which had been shown to be involved in NADP(H) binding in previous studies (Geissler *et al.*, 1994; Nakanishi *et al.*, 1996; Tanaka *et al.*, 1996). Interestingly, concentrating SDRvv above 10 mg ml^{-1} initiated visible aggregation of the protein, which could be solubilized instantly by addition of NADPH. Notably, the addition of up to 1 m*M* NAD$^+$, NADH or NADP$^+$ proved to be inadequate for solubilization of the SDRvv aggregates.

Prior to setting up crystallization drops, the protein solutions were centrifuged for 30 min at 20 000*g* (at 277 K). Initial crystallization trials were performed at 293 K in 96-well dual-drop MRC crystallization plates (Jena Bioscience) using the following commercially available sparse-matrix screens: Crystal Screen, Crystal Screen 2, Index, PEG/Ion and PEG/Ion 2 (Hampton Research). Each well was filled with 70 µl of the corresponding reservoir solution, while the drops were set up using a Mosquito crystallization robot (TTP LabTech) by mixing equal volumes (100 nl) of protein and precipitant solution. The initial screens identified 15 crystallization hits, which were characterized by the presence of 20–25%(*w*/*v*) low-molecular-weight polyethylene glycol. Of these, two promising leads, 0.2 *M* ammonium acetate, 0.1 *M* bis-Tris pH 6.5, 25% PEG 3350 (condition *A*; Fig. 1*a*) and 0.1 *M* bis-Tris pH 6.5, 20% PEG 5000 (condition *B*), which already produced suitably sized crystals within 2 d, were further optimized by varying the pH as a function of the PEG concentration and *vice versa*. For crystals obtained using condition *A* this approach did not improve crystal growth or the X-ray diffraction quality of the crystals. Optimization of condition *B* led to growth of well defined triangular crystals in addition to the generally observed lamelliform beam-shaped crystals (Fig. 1*b*). The triangular-shaped SDRvv crystals obtained using 0.1 *M* bis-Tris pH 6.5, 18% PEG 5000 exhibited better diffraction capacity and generally diffracted to Bragg spacings of 4–2.5 Å. However, a single crystal diffracted to 1.80 Å and led to the reported data set.

2.3.1. Data collection. Crystals were transferred into a drop of mother liquor using a nylon loop (Hampton Research) mounted on a SPINE standard cryocap (Molecular Dimensions). Subsequently, the crystals were cryoprotected by gradually adding an equal volume of mother liquor supplemented with 40%(*v*/*v*) PEG 400. The crystals were then flash-cooled directly in liquid nitrogen and loaded into SPINE/ESRF pucks for storage and transport. Data sets were collected from the two crystal forms, SDRvv-*A* and SDSRvv-*B*, to 2.35 and 1.80 Å resolution, respectively. The corresponding data-set statistics are summarized in Table 1.

2.3.2. Data analysis. Both crystal forms belonged to the monoclinic space group $P2_1$ and both were predicted to contain one SDRvv tetramer per asymmetric unit on the basis of their calculated Matthews coefficients (Table 1), resulting in solvent contents of 46 and 50% for SDRvv-*A* and SDRvv-*B*, respectively. The structure of SDRvv could be determined by maximum-likelihood molecular replacement (MR) as implemented in *Phaser* (McCoy *et al.*, 2007). A monomeric search model based on the structure of 3-oxoacyl-(acyl carrier protein) reductase from *Thermotoga maritima* (PDB entry 1o5i; Joint Center for Structural Genomics, unpublished work) was created by *CHAINSAW* (Stein, 2008) by pruning nonconserved residues to the C$^\gamma$ atom. The ensuing MR search for SDRvv-*A* resulted in the consecutive placement of four copies of the search model, creating a tetrameric assembly as in the homologous *T. maritima* structure. The reported *Z* scores for the translation function (TFZ) were 3.8 (TFZ$_1$), 8.0 (TFZ$_2$), 7.6 (TFZ$_3$) and 10.1 (TFZ$_4$). Subsequently, a solution for SDRvv-*B* was easily obtained using the MR solution of SDRvv-*A*. Analysis of the crystal packing and the quality of the calculated electron-density maps indicated that the MR solutions found were correct. Initial rigid-body and coordinate refinement in *PHENIX* (Adams *et al.*, 2010) showed that in contrast to SDRvv-*A*, SDRvv-*B* displayed strong and contiguous unbiased difference density for the cofactor at the SDRvv active site (Fig. 2). SDRvv-*A* crystals therefore appeared to contain protein crystallized in the unbound state, despite the fact that SDRvv–

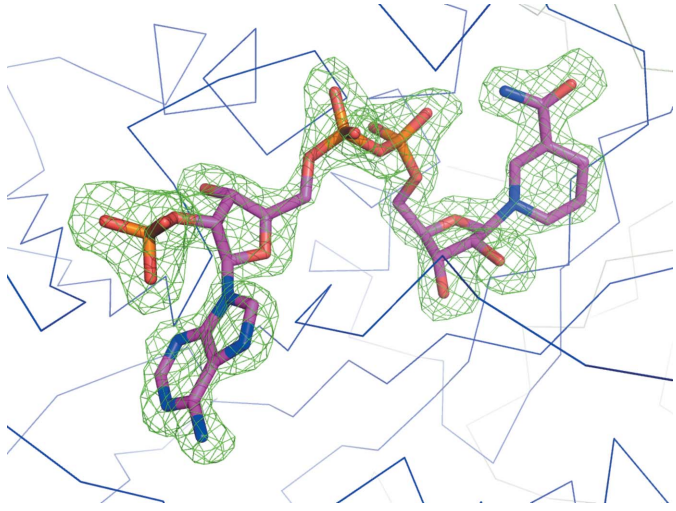

Figure 2
The unbiased difference density map ($F_o - F_c$) in the vicinity of the NADP(H) cofactor, contoured at +3σ, confirms the presence of a bound cofactor in SDRvv-*B*. An NADPH molecule was manually docked in the positive difference density using *Coot*. The figure was generated by carving the map with a radius of 3.0 Å around the NADPH molecule in *PyMOL* (Schrödinger LLC).

NADPH complex molecules prevailed at the beginning of the crystallization experiment. Therefore, the apo crystals strongly suggest a crystal packing in which the flexible motif (*i.e.* 'the substrate-binding loop') shielding the cofactor-binding site from the solvent in SDR family members is not restrained, allowing mass-action-driven cofactor exchange. As NADPH spontaneously and rapidly oxidizes to $NADP^+$, crystal growth takes place in a continuously changing environment that contains increasing amounts of $NADP^+$ at the expense of NADPH. Hence, the SDRvv active sites in SDRvv-*A* only become empty when the developing amounts of $NADP^+$ (up to 1 m*M*) are not high enough to saturate the protein, *i.e.* implying a significant (greater than tenfold) difference in the affinity of SDRvv for NADPH compared with $NADP^+$. Such a scenario implies that crystal contacts fix the substrate-binding loop in the cofactor-binding conformation in SDRvv-*B* crystals and that the bound cofactor therefore retains its reduced form during crystal growth.

While it remains uncertain whether SDRvv represents a catalytically competent reductase, the co-occurrence of SDRvv homologues with divergently transcribed LysR-type transcriptional regulators in *Vibrio* species and other bacterial pathogens (Szklarczyk *et al.*, 2010) establishes the possibility that SDRvv-like proteins fulfil a role in redox control of transcription.

GB is a research fellow of the 'Instituut voor de Aanmoediging van Innovatie door Wetenschap en Technologie in Vlaanderen' (IWT). BV and KV were supported by research fellowships from the Research Foundation Flanders, Belgium (FWO). We gratefully acknowledge beam-time allocation and technical support provided at the French National Synchrotron Facility (SOLEIL) and the Swiss Light Source (SLS). We would like to thank Laurence Van Oudenhove (L-ProBE Unit for Mass Spectrometry and Proteomics) for the peptide mass fingerprinting.

References

Adams, P. D. *et al.* (2010). *Acta Cryst.* D**66**, 213–221.
Diederichs, K. & Karplus, P. A. (1997). *Nature Struct. Biol.* **4**, 269–275.
Filling, C., Berndt, K. D., Benach, J., Knapp, S., Prozorovski, T., Nordling, E., Ladenstein, R., Jörnvall, H. & Oppermann, U. (2002). *J. Biol. Chem.* **277**, 25677–25684.
Geissler, W. M., Davis, D. L., Wu, L., Bradshaw, K. D., Patel, S., Mendonca, B. B., Elliston, K. O., Wilson, J. D., Russell, D. W. & Andersson, S. (1994). *Nature Genet.* **7**, 34–39.
Hoffmann, F. & Maser, E. (2007). *Drug Metab. Rev.* **39**, 87–144.
Jones, M. K. & Oliver, J. D. (2009). *Infect. Immun.* **77**, 1723–1733.
Kallberg, Y., Oppermann, U., Jörnvall, H. & Persson, B. (2002). *Protein Sci.* **11**, 636–641.
Kantardjieff, K. A. & Rupp, B. (2003). *Protein Sci.* **12**, 1865–1871.
Kavanagh, K. L., Jörnvall, H., Persson, B. & Oppermann, U. (2008). *Cell. Mol. Life Sci.* **65**, 3895–3906.
Matthews, B. W. (1968). *J. Mol. Biol.* **33**, 491–497.
McCoy, A. J., Grosse-Kunstleve, R. W., Adams, P. D., Winn, M. D., Storoni, L. C. & Read, R. J. (2007). *J. Appl. Cryst.* **40**, 658–674.
Nakanishi, M., Kakumoto, M., Matsuura, K., Deyashiki, Y., Tanaka, N., Nonaka, T., Mitsui, Y. & Hara, A. (1996). *J. Biochem.* **120**, 257–263.
Oppermann, U. C. & Maser, E. (2000). *Toxicology*, **144**, 71–81.
Price, A. C., Zhang, Y.-M., Rock, C. O. & White, S. M. (2004). *Structure*, **12**, 417–428.
Rossmann, M. G., Moras, D. & Olsen, K. W. (1974). *Nature (London)*, **250**, 194–199.
Stein, N. (2008). *J. Appl. Cryst.* **41**, 641–643.
Szklarczyk, D., Franceschini, A., Kuhn, M., Simonovic, M., Roth, A., Minguez, P., Doerks, T., Stark, M., Muller, J., Bork, P., Jensen, L. J. & von Mering, C. (2010). *Nucleic Acids Res.* **39**, D561–568.
Tanaka, N., Nonaka, T., Nakanishi, M., Deyashiki, Y., Hara, A. & Mitsui, Y. (1996). *Structure*, **4**, 33–45.